Research Square

Preprints are preliminary reports that have not undergone peer review.
They should not be considered conclusive, used to inform clinical practice,
or referenced by the media as validated information.

Correcting droplet–flame interactions in an artificially thickened turbulent lifted flame

Satoshi Kuramoto

satoshi.kuramoto@usp.br

Universidade de São Paulo

Luís Eduardo de Albuquerque Paixão Freire de Carvalho

Universidade de São Paulo

Louis Dreßler

Technische Universität Darmstadt

Amsini Sadiki

Technische Universität Darmstadt

Fernando Luiz Sacomano Filho

Universidade de São Paulo

Research Article

Keywords: Computational Fluid Dynamic, Large Eddy Simulation, Artificially Thickened Flame, Flamelet Generated Manifold, Spray flame

Posted Date: July 27th, 2026

DOI: https://doi.org/10.21203/rs.3.rs-10284891/v1

License: This work is licensed under a Creative Commons Attribution 4.0 International License.
Read Full License

Additional Declarations: No competing interests reported.

Correcting droplet–flame interactions in an artificially thickened turbulent lifted flame

Satoshi Kuramoto[1*],
Luís Eduardo de Albuquerque Paixão e Freire de Carvalho[1],
Louis Dreßler[2], Amsini Sadiki[2, 3],
Fernando Luiz Sacomano Filho[1,4*]

[1]Department of Mechanical Engineering, Escola Politécnica da Universidade de São Paulo, Av. Prof. Mello Moraes, 2231, São Paulo, 05508-030, São Paulo, Brazil.
[2]Institute for Simulation of Reactive Thermo-Fluid Systems, Technische Universität Darmstadt, Otto-Berndt-Straße 3, Darmstadt, 64287, Hessen, Germany.
[3]Laboratoire de Modélisation Mécanique, Energétique et Matériaux, Institut Supérieur des Techniques Appliquées (ISTA-Kinshasa), Avenue Aérodrome N◦3930, Kinshasa, BP 6593, Commune de Barumbu, Democratic Republic of the Congo.
[4]Research Centre for Greenhouse Gas Innovation, Universidade de São Paulo, Av. Prof. Mello Moraes, 2231, São Paulo, 05508-030, São Paulo, Brazil.

*Corresponding author(s). E-mail(s): satoshi.kuramoto@usp.br; fernando.sacomano@usp.br;
Contributing authors: luis.eduardo.carvalho@usp.br; dressler@rsm.tu-darmstadt.de; sadiki@rsm.tu-darmstadt.de;

Abstract

Large Eddy Simulations are conducted for the Coria Rouen n-heptane spray jet burner, featuring an unconfined geometry with a non-swirling air co-flow. The resulting lifted flame exhibits a complex structure governed by strongly coupled interactions of turbulence, droplet evaporation, and chemical reactions. The multiphase flow is modeled using an Eulerian–Lagrangian approach to provide detailed insight into turbulent spray flame structures. Simulations are performed

with the finite volume open-source code OpenFOAM. The combustion chemistry is represented using a Flamelet Generated Manifold (FGM) approach, whereas turbulence-chemistry interaction is modeled with Artificially Thickened Flame (ATF) and a power law efficiency function. Two correction strategies, referred to as standard and projection methods, are implemented to address the interaction between the artificially thickened flame and liquid droplets. Departing from a successful validation process of the employed models, the obtained results complement previous investigations conducted for turbulent spray flames stabilized by pilot flames. The importance of the correction strategies for the accurate prediction of lifted spray flames is clearly identified. Both approaches deliver in general similar results, but the projection approach is presented as the most suitable due to the evaporation rates observed on the droplets, with closer agreement with the reference experiment, and furthermore the better theoretical consistency.

Keywords: Computational Fluid Dynamic, Large Eddy Simulation, Artificially Thickened Flame, Flamelet Generated Manifold, Spray flame

1 Introduction

The usage of liquid fuels in modern engines and combustors usually encompasses the formation of turbulent spray flames. Modeling such a combustion process by means of Computational Fluid Dynamics (CFD) tools with the LES approach allows to characterize the diverse underlying and strongly coupled phenomena. In specific to turbulent spray flames, typically used models may conflict to each other in terms of the basic hypothesis embedded into them when spatial resolution is increased. This occurs when the grid resolution approaches that of the reaction zone width and the minimum control volume size no longer attend the Particle Source in Cell (PSIC) approach [1] applied in the description of disperse flows. When this is not carefully watched, simulation outcomes may be distorted.

The particle source in cell approach is a common assumption in the modeling of turbulent spray flames [2–41] as it circumvents the need for describing the boundary of immersed liquid droplets moving into the gaseous flow [42]. This approach is used in a broad spectrum of disperse flows simulations, which includes the simulation of flames propagating in droplet mists [43–46], turbulent spray flames [2–39], engines [40, 41] etc. Commonly, most studies found in the literature dealing with turbulent spray combustion do not explicitly mention whether any treatment is applied to satisfy the basic assumptions of the PSIC approach. Nevertheless, Portela and Oliemans [47] have shown, for highly-resolved LES with two-way coupling, deviations from these assumptions may not always affect the particle-laden flow.

In the literature, turbulent spray combustion is commonly modeled using presumed PDF approaches [6, 7, 19, 27], transported PDF methods [11, 15–17, 26, 27], Conditional Moment Closure (CMC) [18, 34, 35], Filtered Tabulated Chemistry for Large Eddy Simulation (FTACLES) [8, 9, 25, 48, 49], and the Artificially Thickened Flame (ATF) method [3, 10, 20, 28–30, 50–53]. Among the main models used to describe

turbulent spray combustion, the ATF method offers an important advantage in ensuring compliance with the PSIC requirements and it avoids excessive mesh refinement below the PSIC resolution limit for the reaction zone, thereby ensuring PSIC validity. However, ATF introduces distortions in the interaction between artificially thickened reaction zones and the fuel droplets.

The ATF was primarily designed for premixed gaseous flames, in which by artificially thickening a flame front, the flame propagation can be resolved in the computational grid [54]. Over time, the ATF was extended to spray flames [3, 28], which involve liquid fuel droplets that evaporate and create a flammable mixture. In this context, the artificial thickening of the flame introduces additional challenges. The modified temperature and species gradients throughout the reaction zone affect the evaporation rates of the droplets, which subsequently affect the mixture composition. These effects can influence the droplet lifetime, flame structure, and combustion dynamics, introducing uncertainties. Therefore, while the ATF can be applied to sprays, its implementation requires a correction considering the droplet–flame interactions to account for the changes by the artificial thickening.

Strategies to account for the effects of artificial thickening on the droplets were investigated in the literature [2, 10, 28]. In Sacomano Filho et al. [28], an investigation was conducted within the Eulerian-Lagrangian framework for a piloted lean partially prevaporized flame. Herein, mass and heat transfer rates were corrected by the Eulerian thickening factor computed at droplet location. No directional consideration was done in this approach. Similarly, Boileau [2] considered a similar process, but within the Eulerian-Eulerian framework. In order to preserve the flame speed in the resulting approach, Boileau [2] did also include a correction in the Eulerian drag. Directional effects are first introduced by Dressler et al. [10], where they studied numerically a turbulent spray jet flame and implemented other two correction methods.

In previous studies [10, 28], the ATF was investigated in the context of jet flames stabilized by pilot flames. To broaden and generalize the applicability of the ATF - particularly due to its inherently desirable PSIC feature - this work focuses on lifted flames. In contrast to flames stabilized by pilot flames, lifted flames exhibit distinct stabilization mechanisms and encompass multiple combustion regimes within a single configuration, making them more representative of industrial applications. Furthermore, this configuration enables the extension of the previous investigations on piloted flames by Dressler et al. [10], thereby addressing an open need in the literature.

The correction models applied to represent the droplet-flame interaction within the ATF context and the PSIC approach (i.e. those proposed in [10, 28]) are evaluated to identify the most physically relevant and representative approach for simulating a generalized flame configuration. The models are applied to a real setup, namely the CORIA Spray Burner, where simulation results are compared with experimental data to assess different strategies for correcting evaporation models. In this study, the objective is not to achieve exact agreement between simulation and experimental results. Instead, the focus is on evaluating the behavior of the correction models within the context of lifted flames. To this end, the chosen configuration allows for a consistent and physically meaningful analysis of the simulation outcomes. This approach emphasizes the understanding of underlying mechanisms and trends specific to lifted flame

stabilization, rather than strict quantitative matching with experimental data. The study evaluates the impact of the corrections on droplet evaporation and their subsequent effects on flame structure, with particular emphasis on assessing their necessity and significance.

Following this introduction, the employed models used to perform our simulations are briefly described. In the sequel, the experimental and the numerical setup are detailed. More place is reserved to the presentation of the obtained results in section 4, in which the results achieved for the turbulent spray flame are systematically exposed and discussed. At the end, final remarks are summarized and a brief outline is presented.

2 Model

An Eulerian–Lagrangian approach was adopted to represent the two-phase flow. The gas phase is treated as a continuous medium using an Eulerian formulation, while the liquid phase consists of dispersed droplets tracked within a Lagrangian framework. Although both phases are treated separately, a full two-way coupling between the phases is considered.

The numerical analyses are carried out using the open-source finite-volume solver OpenFOAM [55], which has been adapted to include the low-Mach-number formulation proposed by Ries et al. [56]. Additional functionalities have been incorporated subsequently by Dressler et al. [10].

2.1 Gas phase

The turbulent motions of the carrier phase are modeled within the LES framework, considering the transport equations for mass, momentum, mixture fraction, and progress variable. The unresolved turbulent fluxes, represented by the Subgrid Scale (SGS) stress tensor, are modeled using the sigma eddy-viscosity model proposed by Toda et al. [57], which has been shown to adapt dynamically to variations in the local strain rate.

In the applied FGM database [58, 59], the chemical state is reconstructed using two control variables: the mixture fraction Z and the reaction progress variable Y_{PV}. To generate such database, adiabatic and steady freely propagating premixed flamelets are calculated using the solver CHEM1D [60]. It was used the Toluene Primary Reference Fuels (TPRF) kinetic mechanism for the n-heptane of the Polytechnic University of Milan [61–63], with the flammable equivalence ratio varying from 0.48 to 1.97. The transport equations for both variables are expressed within the ATF approach in Eqs. 1 and 2 and the sub grid terms are modeled considering the Reynolds analogy.

$$\frac{\partial \overline{\rho}\widetilde{Z}}{\partial t} + \frac{\partial \overline{\rho}\widetilde{Z}\widetilde{u}_j}{\partial x_j} = \frac{\partial}{\partial x_j}\left(\left(FE\frac{\overline{\mu}}{Sc} + (1-\Omega)\frac{\mu_{sgs}}{Sc_{sgs}}\right)\frac{\partial \widetilde{Z}}{\partial x_j}\right) + \overline{S}_Z \tag{1}$$

$$\frac{\partial \overline{\rho}\widetilde{Y}_{PV}}{\partial t} + \frac{\partial \overline{\rho}\widetilde{Y}_{PV}\widetilde{u}_j}{\partial x_j} = \frac{\partial}{\partial x_j}\left(\left(FE\frac{\overline{\mu}}{Sc} + (1-\Omega)\frac{\mu_{sgs}}{Sc_{sgs}}\right)\frac{\partial \widetilde{Y}_{PV}}{\partial x_j}\right) + \frac{E}{F}\overline{\dot{\omega}}_{PV} \tag{2}$$

The filtered quantities are transported according to the Favre decomposition $\phi = \tilde{\phi} + \phi''$, where $\tilde{\phi} = \overline{\rho\phi}/\overline{\rho}$. In this notation, over-bars and tildes represent respectively spatially and density-weighted filtered quantities, while double primes correspond to subgrid scale fluctuations. Here it is used the index notation, where the variable u_i represents the velocity at the direction i, S is the source term, μ is the dynamic viscosity, Sc is the Schmidt number and ω_{PV} is the source term for the progress variable. In the ATF context, F is the thickening factor, E is the efficiency function and Ω is the flame sensor, used to constrain the thickened region.

The PSIC method is a two-way coupling approach commonly employed in Eulerian–Lagrangian multiphase simulations to represent the interaction between a dispersed and the continuous fluid phase. The influence of the dispersed phase on the carrier flow is accounted for through a source term, $\overline{S}_Z$, added to the mixture fraction equation. The mixture fraction, as formulated by Bilger [64], and the reaction progress variable, defined as Eq. 3, are used to retrieve the thermochemical state during runtime.

$$Y_{PV} = \frac{Y_{CO_2}}{W_{CO_2}} + \frac{Y_{CO}}{2W_{CO}} + \frac{Y_{H_2O}}{2W_{H_2O}} \tag{3}$$

The efficiency function proposed by Charlette et al. [65, 66] (Eq. 4) is applied to account for subgrid-scale wrinkling and restore the actual turbulence–flame interaction. To keep the present investigations aligned with those conducted by Dressler et al. [10], the parameter β used in the efficiency function is here set to 0.5.

$$E = \frac{s_t}{s_l^0} = \left(1 + \min\left(\frac{\Delta}{\delta_l^0}, \Gamma\frac{u'_\Delta}{s_l^0}\right)\right)^\beta \tag{4}$$

The thickening procedure is applied within the reaction zone, identified using the flame sensor Ω. In this study, the Aschmoneit's formulation [67] is employed, which combines the progress variable (likewise Durand and Polifke [52]) and its source term to detect reaction zones.

2.2 Liquid phase

The dynamics of the considered non-rotating droplets are determined solely by drag, gravity, and buoyancy forces. Heat and mass transfer on droplets are modeled according to the Abramzon-Sirignano model [68], following the formulation proposed by Miller et al. [69]. An additional correction term, F_{eff}, is included to model the influence of flame thickening on the dispersed droplets. The mass and heat transfer rates are described, respectively, by Eqs. 5 and 6.

In this context, T_g is the temperature of the gas phase and T_d the temperature of the droplet. The variables Nu, Sh, Sc, and Pr are the dimensionless Nusselt, Sherwood, Schmidt and Prandtl numbers, respectively. The variable f_2, θ_1, τ_d, and H_M are the correction factor due to evaporation, the ratio of the gaseous and liquid specific sensible heat, the droplet relaxation time and the specific driving potential for mass transfer, respectively. Nusselt and Sherwood numbers are calculated by Ranz and Marshall empirical correlations. Additional details are found in [69].

$$\dot{m}_d = \frac{dm_d}{dt} = -\frac{1}{F_{eff}} \frac{1}{3} \frac{Sh}{Sc} \frac{m_d}{\tau_d} H_M \tag{5}$$

$$\dot{T}_d = \frac{dT_d}{dt} = \frac{1}{F_{eff}} \frac{f_2 Nu}{3Pr} \frac{\theta_1}{\tau_d} (T_g - T_d) + \frac{L_{vap}}{c_{p_{liq}}} \frac{\dot{m}_d}{m_d} \tag{6}$$

To examine the interaction between the liquid phase and the flame, both the standard and the projection correction methods proposed respectively by Sacomano Filho et al. [28] (see Eq. 7) and Dressler et al. [10] (see Eq. 8) are considered. The correction methods adjust the droplet heat and mass transfer rates to recover the appropriate heat and mass transfer rates while droplets are traveling into the artificially thickened scalar fields. This correction strategy provides a consistent and reliable framework for studying droplet–flame interactions within the PSIC approach.

$$F_{eff,std} = F \tag{7}$$

$$F_{eff,prj} = 1 + \left| \frac{\partial Y_{PV}/\partial x_j}{|\partial Y_{PV}/\partial x_j|} \frac{u_j}{|u_j|} \right| (F - 1) \tag{8}$$

The models used in this study were carefully chosen in order to provide a physical consistent tool to evaluate a lifted spray flame. It is expected that the local thickening of the flame modifies the droplet dynamics. The evaporation rates should consequently be affected, triggering a cascade of interactions: additional fuel is released into the gas phase, the local mixture composition changes, and the combustion process itself is subsequently altered. This interaction between phases are analyzed in the next sections.

3 Experimental and Numerical Setups

In this section, the experimental setup is described and the main characteristics of the burner, the experimental techniques used to extract data, and the main aspects of the flame are presented. To assess the simulations, the mesh is described and the main regions are pointed out in the sequel. Next, important aspects of the numerical setup are introduced.

3.1 CORIA Spray Burner simulations

The non-swirling, lifted flame of the CORIA spray burner setup was chosen as a reference for the conducted simulations in turbulent flow. This setup offers an important configuration to assess the impact of the different correction approaches applied to the interaction of droplets and the thickened flame. As the flame is lifted and droplets are able to cross reaction zones, the effects of the investigated corrections are expected to be pronounced, at least on spray characteristics. Exactly by the same aspect, the resulting flame exhibits premixed and diffusion flame modes simultaneously, which restricts the capability of the ATF and FGM approaches on rigorous capturing flame characteristics. As already mentioned on the introduction of this manuscript, the ATF was developed to described premixed flames, and the employed efficiency function

as well. With this in mind, the employed FGM was also constructed with premixed flamelets preserving the consistency of the method. Therefore, the employed method cannot rigorously describe eventual reaction zones burning in the diffusion flame mode. Therefore, we focus on the flame stabilization region, which is predominantly governed by the premixed flame mode. This does not affect the objective of the present study to evaluate the behavior of the droplet-flame interaction models within the context of lifted flames and the PSIC approach.

3.2 Numerical setup

The numerical simulations follows the experimental configuration, where measurements were carried out in an atmospheric open ambient, with no confinement, no swirling flow at temperature and pressure of 298 K and 1 atm. The nozzle exit features an annular geometry, characterized by inner and outer diameters of 9 and 20 mm, respectively. The burner operates with an air flow rate of 6 g/s, with an average velocity at the nozzle of 20.21 m/s and hydraulic Reynolds number of 14300, while n-heptane is injected at a rate of 0.28 g/s through a DANFOSS hollow cone fuel injector. The flame is lifted, indicating that the combustion zone is positioned above the nozzle exit, where the fuel has partially pre-evaporated and mixed with air to reach a sufficient flammable mixture allowing ignition and stabilization [22, 32, 36–38, 70].

The experimental database, obtained from reference experiments conducted at INSA Rouen Normandie, includes Phase Doppler Anemometry (PDA) measurements of the droplet velocity and diameter, OH Planar Laser-Induced Fluorescence (OH-PLIF) imaging, droplet temperature measurements using the Global Rainbow Refractometry Technique (GRT), as well as simultaneous high-speed OH-PLIF and high-speed Particle Image Velocimetry (PIV) measurements [22, 32, 36–38, 70].

Earlier experimental investigations [38] have identified and characterized the various regions within the flame as illustrated in Fig. 1, which was obtained from the instantaneous plot of the temperature of the gas phase achieved from the LES conducted in the present work. The leading edge (LE), located near the injector, connects the inner and outer reaction zones (IRZ and ORZ). The thicknesses of OH layers in experiments reveal the presence of two simultaneous combustion modes. The ORZ shows a stable, but thick OH layer, indicating the diffusion flame mode, whereas the IRZ presents a thinner, highly wrinkled flame influenced by the air jet, indicating a turbulent flame driven by premixing of reactants. As mentioned by Sitte and Mastorakos [33], the ORZ behaves as a quasi-steady diffusion flame, while the IRZ exhibits partially premixed characteristics. The LE is mostly premixed, exhibiting a thin OH layer.

The modeling of the atomization process is beyond the scope of the present study. Herein, we follow the premise of employing strategies already assumed in other studies to better communicate our results with those obtained by pairs. Hence, as done for the exponent of the efficiency function in Eq. 4, the injection of spray droplets in the computational domain follows the method adopted by Both [4], in which the positions and initial velocities of droplets are prescribed in a specific region. Again, this choice ensures consistency with previous works [4, 33] bringing them in a same framework.

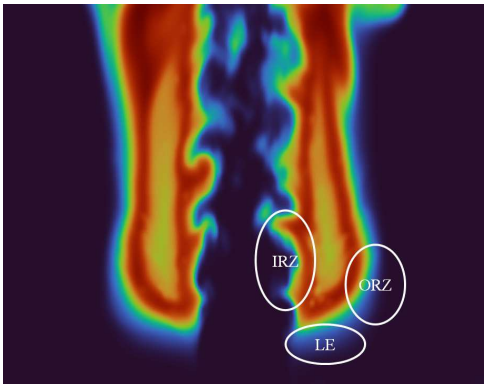


Fig. 1 Instantaneous plot of the temperature obtained from the LES conducted in the present work with the projected correction method. The leading edge (LE) is located at the most lower part of the flame, between the inner reaction zone (IRZ) and the outer reaction zone (ORZ).

3.2.1 Mesh, initial and boundary conditions

The computational domain consists in a mesh with a height of 220 mm and a diameter of 260 mm. The mesh was created with hexahedral cells in its majority, with a few prism in transitional zones, with approximately 4.8 million cells in total. The annular non-swirling air inlet (at the bottom part of the burner) has internal and external diameters of 9 mm and 20 mm and it is followed by air ducts supplied with 18 radial non-swirling vanes. Figure 2 shows a quarter of the geometry meshed. The bottom part of the mesh includes the plenum and the vanes. The upper region, after the vanes, lodges the main phenomena of the simulations, with a height of 85 mm, therefore requiring an uniform discretization (cells with 0.2 mm on average in its central region). The mesh was designed to obtain a regular discretization and to attenuate numerical artifacts in the stabilization zone of the flame. This region comprehends the detailed screening performed with experimental measurements, allowing comparisons between simulation results and experimental data.

A detailed view of the vertical cross-section is shown in the right side of Fig. 2. The central region (central circle, radius from 0 to 18 mm) corresponds to the IRZ and it is fully refined in the radial direction. The greater circumference (outer annulus, radius from 18 to 50 mm) represent the ORZ, where a uniform cell size is applied in the radial direction as seen in the bisector plane. The mesh indicated as the "FTT volume" in Fig. 2 was specifically designed as the data-extraction region and were generated to minimize cell distortion along the two principal axes (x and y) of the model.

The origin of the computational domain is defined at the spray injection point, positioned immediately above the vanes along the main axis of the burner (marked spot on the left side of Fig. 2). From this point, the liquid phase is introduced into the simulation as spray droplets.

In this configuration, the fuel is injected in liquid form, with the entire mass flow initially concentrated at the nozzle orifice. For $z > 5$ mm, droplets are assumed spherical and the spray dilute, allowing droplet–droplet interactions to be neglected. The numerical spray has an average of 2.2 million per second parcels being injected, with

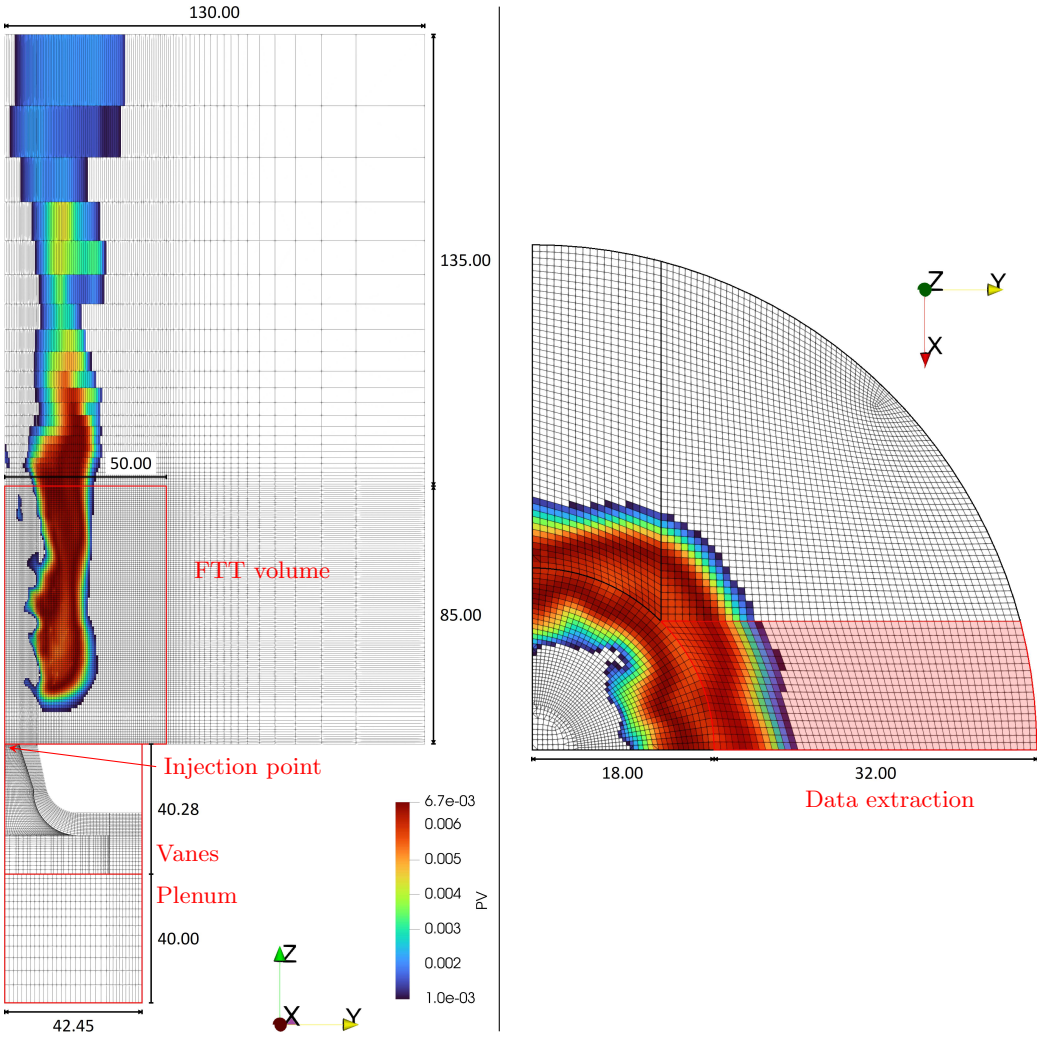


Fig. 2 Mesh of a quarter of the geometry. On the left, a horizontal sectional view. The "FTT volume", outlined in red, shows the volume used to calculate the FTT, and below the vanes connecting the plenum with the combustion region, both also outlined in red. On the right, a vertical cross section extracted at height of 10 mm and radius up to 50 mm. The data extraction region, outlined in red, is where all the data was extracted from simulations. It has cells with better quality and less distortions. All indicated dimensions are in mm.

a mean angle of 40 degrees and velocity of 32.88 m/s. A Rosin Rammler distribution is used to set the values for diameters, with minimum and maximum diameters of 3.5 and 70 µm and average diameter of 35.062 µm and an exponential parameter of 3.45. The parcels are separated in large and small diameters (70 and 20 µm, respectively), with angles of injection between 20 and 60 degrees for small particles and between 35 and 42 for large ones. Along the simulations, it was injected around 1.5 million parcels.

In regard of the gaseous phase, the air entry in the lower part of the plenum has a flow of 6 g/s, with a zero gradient condition for pressure. The co-flow (at $z = 0$ mm and $r > 70$ mm) has a constant velocity input of 0.5 m/s, with also zero gradient condition for pressure. The free domain boundaries are modeled with zero gradient condition for velocity and zero total pressure. Wall conditions are used for the walls of the plenum and the surface of the burner at $z = 0$ mm and $r < 70$ mm.

The simulations were started with the injection of n-heptane under non-reacting conditions, allowing the fuel to evaporate and form a mixture suitable for ignition. This initialization phase last 0.1 s, ensuring adequate conditions for flame ignition. The simulations were run for 1.5 flow through time (FTT) to initialize the flow field, followed by the time averaging for 4.5 FTT to reach a statistical convergence. The FTT was computed using the "FTT volume" indicated in Fig. 2, defined by a height of 85 mm and a diameter of 100 mm. Using the previously defined mass flow rate, one FTT corresponds to approximately 0.1318 s.

4 Results

As previously mentioned, a great extension of this manuscript is dedicated to the presentation of the obtained results. In the follow, the general characteristics of the flame are described, in order to situate the reader about its main aspects. More detailed results are presented from sections 4.2 to 4.3.

Altogether, three simulations were performed to assess the impact of different correction approaches. The first simulation was conducted without any correction and serves as the baseline for comparison (reference case). The second employed the standard correction method [28], while the third used the projected correction method [10]. Both correction strategies are evaluated relative to the reference case, and a direct comparison between the standard and projected methods is also performed. The non-corrected reference case will be denoted as REF, while the standard and projected correction will de denoted as STD and PRJ, respectively.

It is important to mention that a non-reactive simulation was conducted to successfully validate the entire numerical setup (see supplementary material). Good adherence between numerical and experimental data was observed, providing a consistent basis for its application to reactive flows.

4.1 General characteristics of the flame

The instantaneous results for the REF case are presented in Fig. 3, in which the OH regions delineate the flame. enveloped by the regions with high concentration of OH, the elevated CO concentrations indicate incomplete oxidation. The fuel-rich regions, expressed in terms of mixture fraction ($Z > 0.062$), contain significant amounts of partially oxidized species, evidencing the progressive conversion of fuel before complete combustion. Due to the axisymmetric structure of the flame, this partially oxidized zone assumes a toroidal shape. The OH-rich regions are observed to coincide with the reaction zones, which correspond to the regions of highest temperature, while CO is associated with fuel-rich mixtures characterized by lower heat release and temperature.

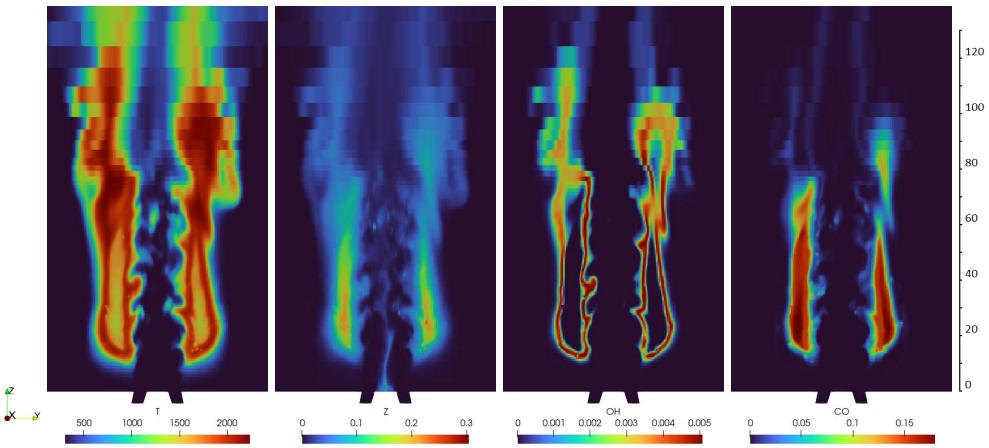


Fig. 3 Instantaneous plots for temperature, mixture fraction, OH and CO, respectively, with the no ATF correction (reference case).

These two species are further addressed, as they are employed in subsequent post-processing.

The inner region of the flame contains the highest fuel concentrations, reaching levels that are overly rich. The fuel then gradually diffuses outward toward the flame contour, where it mixes with the surrounding air and then reaches the outer reaction zone. This mixing reduces the local fuel concentration, bringing it into the flammable range and enabling combustion to occur.

The double flame process was already presented by Shum-Kivan et al. [32], where the authors analyze the combustion regime with the Takeno flame index [71]. This dual behavior is common in lifted spray flames, where local mixing conditions vary spatially, creating regions that transition from premixed to diffusion flame modes. In our simulations, the thicknesses of the OH layers were not significantly different between IRZ and ORZ due to the artificial thickening. It is worth noting that the species mass fractions are directly obtained from the FGM table, which may lead to inaccuracies for the estimation of species variables close to the regions where the diffusion flame mode prevails, i.e. the ORZ. This is an unavoidable consequence of the choice made to construct our FGM table with premixed flamelets. This choice can be justified by the characteristic of LE burning mode, where special attention is given in the present work. This region determines the flame stabilization and defines the flame height, an important flame characteristics. Consequently it influences the region where droplet evaporation primarily occurs, modifies the mixture distribution, and affects the overall flame structure. In this sense, the flame height was regarded as an important parameter for this configuration.

The droplet–flame interactions play an important role in shaping the overall flame structure and the spatial distribution of combustion regimes. This effect is particularly pronounced when comparing the STD and PRJ correction approaches for the ATF. The STD method, which neglects the orientation of parcels or droplets relative to the thickened flame, results in higher correction factors and consequently reduces the heat and mass transfer to droplets within the thickened flame region. In contrast, the PRJ

approach accounts for the orientation of droplet trajectory relative to the flame front, enhancing evaporation and accelerating the formation of a flammable mixture at lower axial positions. The STD correction consistently applies a correction factor equal to F, while the uncorrected case naturally corresponds to a factor of 1 and the PRJ correction produces values ranging between 1 and F, representing an intermediate condition between the two approaches that depends on the angle between the flame front and the droplet trajectory. These differences have a notable effect on local flame dynamics and the evolution of the reaction zones, as illustrated in the time averaged mixture fraction plots in Fig. 4.

The STD correction produces a region with higher fuel concentration on the inner side of the flame compared to the REF approach. This behavior arises because, without correction, evaporation occurs more intensely at the flame front, resulting in locally higher flame propagation speeds and allowing higher penetration of the flame into the jet inner core. In contrast, the corrected approaches reduce the evaporation rate throughout the flame front, resulting in the opposite behavior. However when reducing the evaporation in the jet inner core, more fuel is allowed to evaporate in the hot inner region of the flame, changing the structure of the ORZ.

4.2 Velocity field

The results exhibited in this section show the temporal mean and root-mean-square components at the axial and radial directions of the filtered velocity of the gas phase (Figs. 5 and 6 respectively). The experimental data were obtained using Phase Doppler Anemometry (PDA) as reported in [22, 32, 36–38, 70]. Overall, the numerical results exhibit very good agreement with the corresponding measurements. All simulations show good agreement with the experimental velocity data, remaining within one standard deviation band (represented by the gray area in the plots). In Fig. 5, the impact of the prediction of the flame structure can be noticed. The correction models are able to modify the velocity profile at positions downstream of 16 mm. The PRJ and STD corrections result in a reduction of the carrier-phase velocity, allowing results to be always within the one standard deviation band. Both corrections produce similar results for the carrier phase, indicating that the two approaches yield comparable equivalent behavior for the axial component of droplets velocity. Such results evidentiate the need of applying the correction. It is observed that the corrected approaches yield slightly improved results at higher axial positions, particularly at heights positions downstream of 16 mm.

In Fig. 6, at $z = 5$ mm, it can be observed that the airflow draws the surrounding fluid toward the centerline. This motion is driven by a low-pressure region generated by the jet flow stream, which entrains the co-flow into the flame's center line. This inward motion persists up to approximately z = 16 mm. Since this region is not directly influenced by the flame, all three simulations presented similar results. A major discrepancy is observed at higher axial positions, where the flame is present ($z > 15$ mm), and the experiments indicate a progressive radial spreading of the flame. Although the simulated values remain within the experimental RMS range, the numerical results tend to maintain an approximately constant radial velocity. In

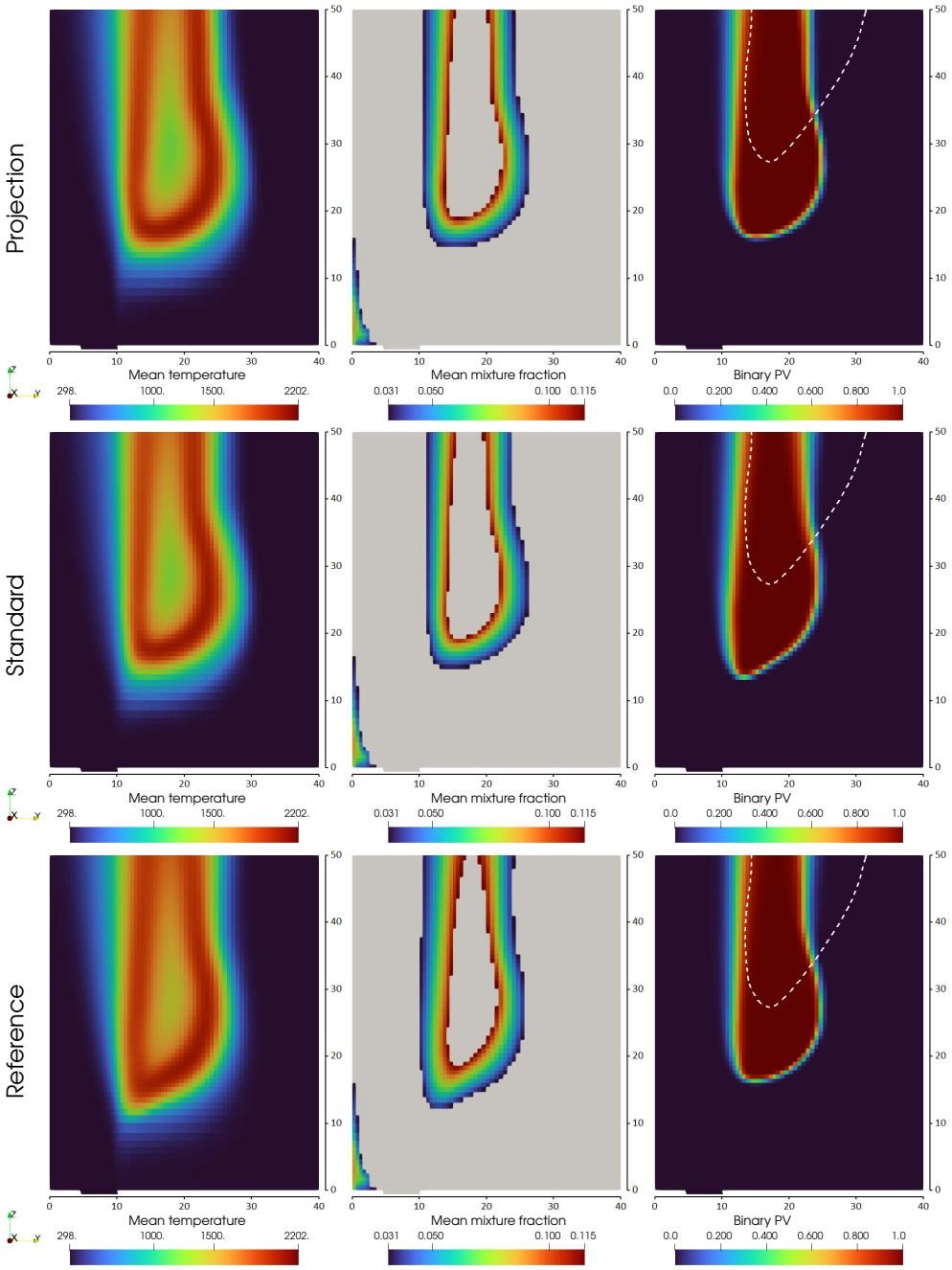


Fig. 4 Time averaged plots for temperature, mixture fraction and binary progress variable in the PRJ, STD and REF cases, respectively. In the binary progress variable plot, the white dashed line correspond to the experimental data contour, extracted from [70]. Dimensions are in mm.

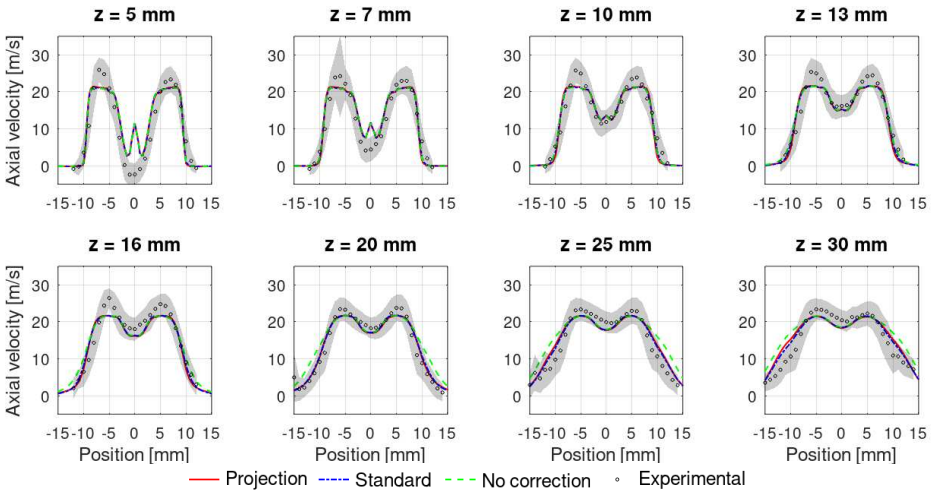


Fig. 5 Mean axial velocity of the carrier phase at different heights (5, 7, 10, 13, 16, 20, 25, 30 mm), evaluated in REF, STD and PRJ cases. Grey zone represents 1 rms.

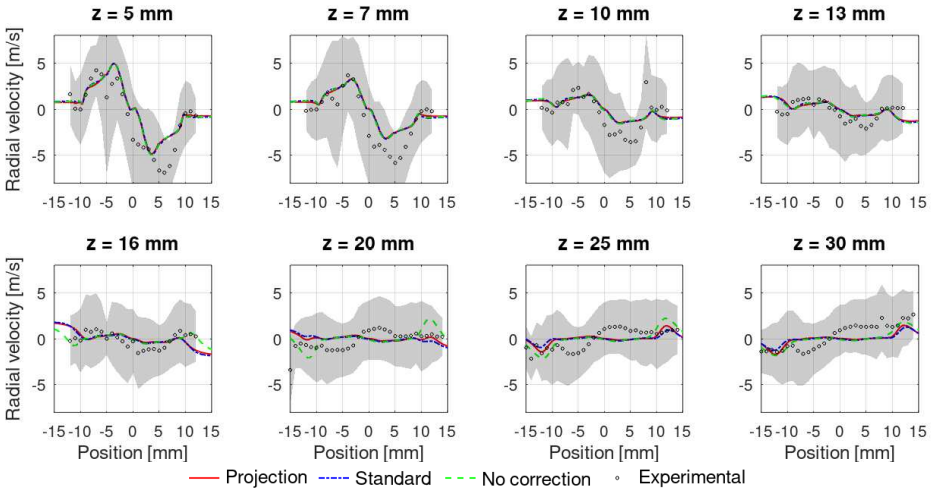


Fig. 6 Mean radial velocity of the carrier phase at different heights (5, 7, 10, 13, 16, 20, 25, 30 mm), evaluated in REF, STD and PRJ cases. Grey zone represents 1 rms.

contrast, the measurements reveal an increasing outward radial velocity, reflecting the gradual lateral expansion of the flame.

The results exhibited in this section show a small impact of each correction model over the Eulerian flow field. The effect of differences in evaporation rates are also small in the final velocity profiles. The velocity profiles of the simulations are very adherent with the experimental result, which is expected in the flow field. Moreover, it is important to validate the next results, in particular the droplet size distribution in the domain.

4.3 Droplets size distribution

Figure 7 presents an instantaneous contour plot of the thickening factor on a slice plane crossing the jet centerline, the instantaneous position of the tracked parcels at time are indicated with white dots. Such a plot is obtained from the simulation conducted with the projection method. The flame thickening alters the evaporation rates according to Eq. 5, in which the term F_{eff} defines a knockdown factor, computed by the STD or the PRJ methods (Eqs. 7 and 8). The spray has a coned shape, which covers a significant portion of flame. The numbered circles on the figure represents points where data was extracted for the subsequent analysis presented in this section. Such data is condensed in Figs. 8, 9, and 10. These figures present droplet size distributions achieved in all simulations in terms of probability density functions (PDF). All of these figures also include experimental data obtained with PDA in [22, 32, 36–38, 70].

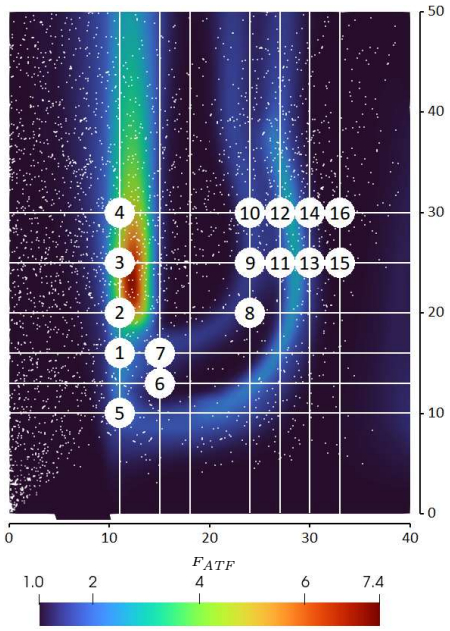


Fig. 7 Plot of the thickening factor with the droplets, in white. Some points marked in the picture correspond to a plot in Figs. 8, 9 and 10.

Three main regions are chosen for this analysis based on the three reaction zones depicted in Fig. 1. The first embraces the IRZ, where the droplets trajectory and the progress variable gradient form a more obtuse angle, causing differences in the droplet evaporation behavior. This can be seen in points 1, 2, 3, and 4 of Fig. 8, where the REF case is offset from the corrected models. It is noted that as long the height increases, the angle between trajectory and gradient of progress variable rises, and the curves for the three cases start to detach from each other. The misalignment between trajectory and gradient of progress variable already points toward a more suitable approach.

Comparing with the experimental values, the PRJ is more adherent than the other methods in the IRZ.

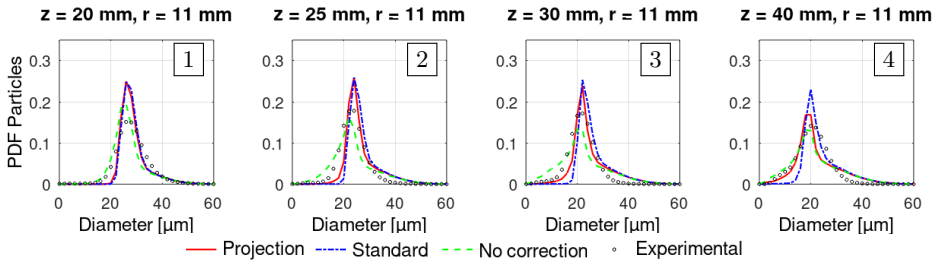


Fig. 8 Probability density function of the diameters of droplets in the reactive flow evaluated in REF, STD and PRJ cases for the IRZ.

For the LE region, the gradient of the progress variable and the trajectories of the droplets form sharper angles. The droplet size distributions of the points 6 and 7 are selected to represent the LE region in Fig. 9. It is evident in Fig. 9 that a correction is also required in this region. However, no clear distinction is noticed between both correction methods in the LE, as expected. In the LE droplets straightly cross the reaction zone, and small directional effects affects the droplet size distributions. Also in Fig. 9 results extracted on the point 5 are presented. In this case, no distinction is noticed among the three models. This occurs since droplets are facing smaller values of the thickening factor.

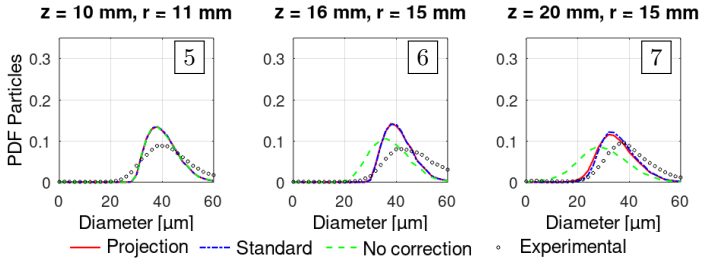


Fig. 9 Probability density function of the diameters of droplets in the reactive flow evaluated in REF, STD and PRJ cases for the LE.

The ORZ region, in contrast to the LE and IRZ, carries the information of a droplet that probably has already crossed the IRZ or LE or even both. Hence, droplet size distributions are results of accumulate interactions with the different flame zones in this region. Another point is the angle of the trajectory with the gradient of progress variable is again misaligned with the ORZ. This influences the PRJ and STD correction methods. However, as angles are not obtuse as for IRZ, the PRJ result tends to do not differ from those of the STD.

When comparing the three methods at the point 10 in Fig. 10, the PRJ presents again a better behavior with the experimental PDF. Although an offset is noticed, both

have similar shapes. The REF method predicts a higher concentration of relatively smaller droplets and a flatter shape when compared to the PRJ results. In contrast to the mono modal shape achieved in all the remaining cases, the STD method shows a bimodal shape with a small peak between 0 μm and 20 μm and a larger one between 30 μm and 40 μm. The inner region of the flame, between the IRZ and ORZ, evaporate the great part of smaller droplets and the bigger droplets survive and remains until they reach the outside, shifting the diameter PDF to bigger diameters. After passing through the ORZ, just some droplets survive with a very narrow interval for the diameter, around 30 µm.

The observed offset among simulation results and experimental data was an expected outcome. In view of the deviations among the simulated and predicted flame shapes, deviations in the PDF at this position are a natural consequence. Furthermore, the point 10 is located in a delicate region of the simulated flames, namely the ORZ. As deduced from experimental measurements [32] the ORZ is dominated by the diffusion flame mode, which is not suitably described by the adopted modeling strategy. The experimental PDF indicates that larger droplets reach the point 10 when compared to simulations. Such deviations are not exclusively caused by deviations among measured and calculated flame shapes, but they are also strongly influenced by the adopted numerical injector.

In all the three regions analyzed, REF results showed high evaporation rates, which suggests the need of a knock down factor and in all three regions. The droplet trajectory and gradient of the progress variable are misaligned, implying that the PRJ method has the most solid theoretical basis for these cases and the better adherence with experimental data.

Is is important to highlight an important characteristic in Fig. 7: a double layer structure is noticed at the ORZ in the contour plots of F_{ATF}. This behavior is a natural consequence of the absence of any clipping for the computation of the thickening factor. This option was made prior to the start of simulations in order to avoid any sharp gradients in the scalar fields and, consequently, numerical overheads. Although there is a flame sensor to limit the artificial thickening, a gradient of the normalized progress variable is formed upstream the LE due to the species diffusion transport, which enables non-zero values of the applied flame sensor (see Aschmoneit's formulation [67]). This has a negligible impact in the overall simulations, but it is sufficient to allow some differentiation among correction models, as seen in terms of the gas temperature in section 4.5.

4.4 Flame height

Although the investigation of the flame high is not a central aspect of this study, results of this quantity are presented here due to its relevance in the context of lifted flames. This quantity is expected to be less sensitive to the investigated models since it is more affected by the mixture and flow conditions arriving the flame front. However, as the correction models affect the mixture formation within the reaction zone, some impact is noticed as such an impact is reflected on the flame speed that influences the definition of the flame height.

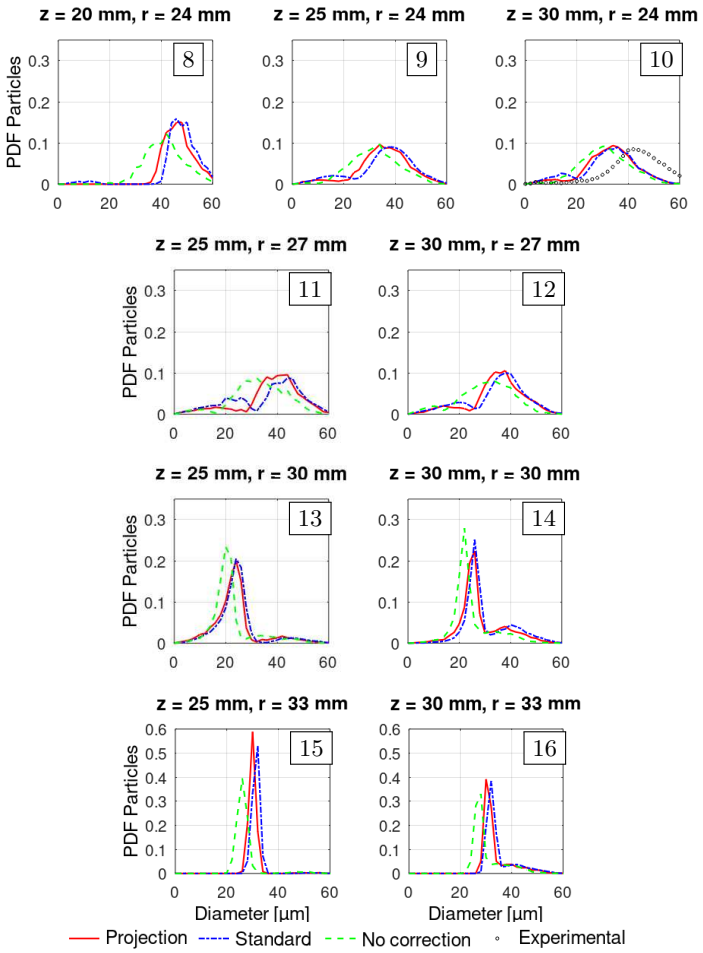


Fig. 10 Probability density function of the diameters of droplets in the reactive flow evaluated in REF, STD and PRJ cases for the ORZ.

The flame height is evaluated using the binary progress variable, which is described subsequently. This variable was selected to ensure consistency with the available experimental data. Mulla et al. [70] proposed a method based on OH-PLIF imaging to identify the flame front using the mass fraction of OH, in which the plots are usually continuous lines that follow the flame front. In these plots, it is discerned a centerline for the mass fraction of OH, that is used as a reference to distinguish the burned (inner) region, that receives the value of unity, and the unburned (outer) region, which is assigned a value of zero. By applying this procedure to 1,500 images and averaging the results, the authors obtained a mean progress variable. The resulting flame shape is indicated on the binary progress variable plots of each simulated case in Fig. 4. To allow a direct comparison with experiments, an analogous methodology used to obtain the experimental mean progress variable was applied using numerical simulation results.

A numerical counterpart for the mean progress variable [70] is proposed. Figure 11 illustrates the procedure used to construct the binary progress variable from the mass fractions of the OH and CO species in the numerical environment. First, the OH mass fraction is used to separate burned and unburned regions (Fig. 11 a). Next, a representative species must be assigned to represent the inner burned region and CO was selected based on agreement with experimental observations (Fig. 11 b). The OH and CO fields are then combined via a weighted sum (Fig. 11 c) and classified into binary values: one for burned, zero for unburned (Fig. 11 d). This field is captured during simulations, and a time average is computed by the solver (Fig. 11 e). The resulting field, referred to here as the binarized progress variable, enables a clear comparison between the numerical procedure and its experimental definition, created from OH-PLIF measurements.

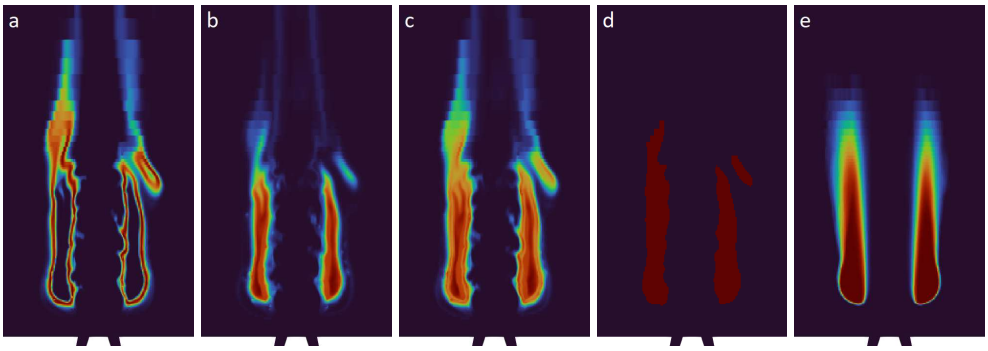


Fig. 11 Illustration of the procedure applied in the numerical simulation to compute the progress variable obtained from experiments in [70]. From left to right, a. mass fraction of OH (Y_{OH}), b. mass fraction of CO (Y_{CO}), c. pondered sum of mass fractions ($2Y_{CO}/Y_{CO,max} + Y_{OH}/Y_{OH,max}$), d. binary PV, e. time averaged binary PV.

Figure 12 and Table 1 present the results obtained from the three conducted simulations for the flame height. The results indicate that, across all simulations, the flame height, defined as the distance between the burner head and the LE, is 15.87 mm for REF, 17.70 mm for STD, and 17.25 mm for PRJ. In these cases, the LE position was defined as the point with the lowest Z coordinate (see Fig. 2), when the averaged binary progress variable reaches 0.99. For comparison, Mulla et al. [70] reported an experimentally measured flame height of 30.63 mm using the mean progress variable in their experiments.

In view of the good agreement noticed in section 4.2 for the velocity field, the observed deviations for the flame height are not expected to derive from the flow momentum. Other aspects may be more important for it, for instance the droplet distribution into the computational domain and the inclusion of heat losses. Hence, by enhancing the numerical injector and including non-adiabatic boundary conditions, a better adherence of the obtained results to the experimental data may be achieved.

The influence of the correction on the LE shape is clearly observed in Fig. 12 and Table 1, and in terms of the contour plots in Fig. 4. The corrected models yield a smoother and more rounded contour of the binarized progress variable, whereas the

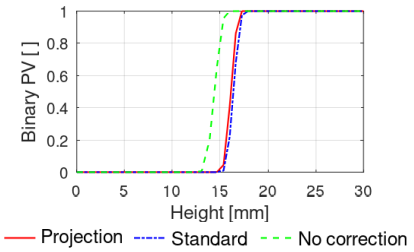


Fig. 12 Plot of binary PV by height. Lines correspond to the binary PV used to evaluate the height of the flame, which is estimated at 99% of its maximum value.

Table 1 Summary of the flame heights [mm] estimated in Fig. 12.

Reference	Standard	Projection
15.87	17.70	17.25

uncorrected model exhibits a markedly sharper interface due to the higher evaporation rate enhances mixture formation in the lower regions of the LE. This is an important result, as the correction factor primarily alters the shape of the flame front, causing it to penetrate further into the flow, which changes the temperature, species, and other fields.

Although the radial positions of the IRZ obtained from simulations demonstrate good adherence with the flame shape obtained from experimental measurements, deviations are evident in Fig. 4. Predictions of the IRZ are also insensitive to the correction models. Deviations are noticed in the flame height and the ORZ. The deviations on the ORZ are a natural consequence of the employed strategy to describe the combustion process (premixed FGM table and the ATF), while those noticed for the LE can be justified by the same arguments used for the deviations noticed in the flame height. As expected, IRZ, which burns in premixed mode, is well predicted by the ATF, while ORZ, which burns in diffusion flame mode, diverges from the ATF predictions.

From the present results, it is clear that the correction is not indispensable for the stability of a lifted flame. Even without correction methods, the lifted flame can exist, showing its high robustness. However, it also affects the flame height, as expected, with higher evaporation rates leading to a reduction in flame height.

4.5 Temperature field

The computed temperature field has been demonstrated to be sensitive to the correction methods, as seen in Fig. 4. As this quantity is obtained from the FGM table, the mixture fraction is analyzed together with the temperature in this section. The mixture fraction is straightly affected by changes of the evaporation rates, as seen through the coupling source term in Eq. 1. For both temperature and mixture fraction, experimental data are unavailable. Hence, results presented here are exclusively obtained from the conducted simulations.

In Fig. 13, radial profiles of the gas temperature are presented at four different axial locations. In these plots, the impact of the different correction methods is quite evident. The temperature amplifies differences between models when compared to the profiles extracted at the same positions in Fig. 14.

Although outside the flammable region (the shaded area on the plots presented in Fig. 14 indicates mixtures between the flammability limits), slight changes in the mixture fraction values are sufficient to cause a strong difference in the temperature profiles at z = 5 mm. The three methods deliver different values for the temperature at this position with the PRJ laying in between the remaining both. At z = 10 mm, both correction methods become close to each other, while the REF is still away from both. This occurs again for mixtures outside the flammability limits. The differences between methods in the region outside the flammability limits is a natural consequence of the absence of any clipping for the computation of the thickening factor, as discussed in section 4.3.

Further downstream, the formed mixture hits flammable compositions and temperatures are able to reach higher values. Temperature differences among uncorrected and corrected droplet-flame interactions reach approximately 500 K at z = 15 mm. As seen in section 4.4, this position coincides with the LE of the REF simulation. The plot at z = 25 mm is found in a region downstream of the LE for all the simulated cases. Herein, a double peak structure for the temperature due to the variation of the mixture fraction as seen in Fig. 14. Approximately between the radial coordinates of 15 mm and 25 mm, the mixture enriches by droplet evaporation at high temperatures in such a way that it comes outside the rich flammability limit. The radial dilution of the mixture allows it to return to a flammable mixture forming the enveloping diffusion flame denoted by ORZ. At both z = 15 mm and z = 25 mm, notable differences are noticed in temperature and mixture fraction profiles.

Differences between STD and PRJ methods are limited to small deviations in the descending part of temperature profiles at z = 10 mm and z = 15 mm. Small deviations are also found at z = 25 mm in the region where the mixture fraction reaches its maximum value. This indicates small sensitivity of the directional effects for the temperature at positions downstream of z = 5mm.

The artificial thickening knock down factor is the single feature that alters the temperature distribution. In the REF case, the evaporation will be more pronounced, which gives the highest temperature, in contrast, the STD case has the highest knock down factor in our evaporation models and this also reflects in the lowest mixture fractions. This highlights the differences in the corrected and non corrected approaches. For far downstream positions of the flame, the temperature curves are prone to converge to the similar values between the three models.

As noticed, the IRZ and ORZ can be clearly identified by the double maximum value regions on each side of the flame, corresponding to the reaction zones where the temperatures reach their highest values. Therefore, the thickening correction models have a negligible effect in the IRZ and ORZ but play a more important role in the LE.

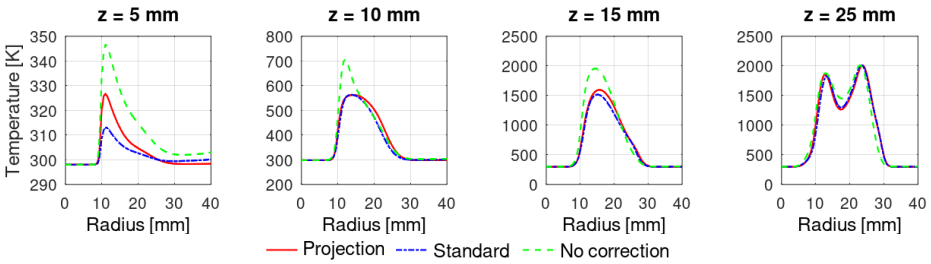


Fig. 13 Average temperature of the carrier phase at different heights, evaluated in REF, STD and PRJ cases.

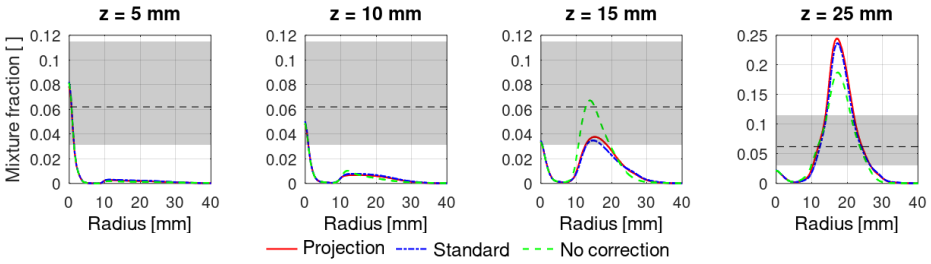


Fig. 14 Average mixture fraction of the carrier phase at different heights, evaluated in REF, STD and PRJ cases. Dashed black line is the stoichiometric ratio and the gray filled region is the flammability zone for the n-heptane.

5 Conclusion

The present study systematically evaluated the behavior of two correction methods developed to characterize droplet-flame interactions within the context of the PSIC approach. Simulations were conducted with the ATF model coupled with a premixed FGM table to calculate a lifted spray flame. Such an evaluation for a lifted flame was an open demand from the investigations presented in Dressler et al. [10]. Both correction methods, denoted here as STD and PRJ are evaluated with a benchmark denoted as REF case. It could be noticed that the inclusion of a correction method is indispensable to recover specific features related to a spray flame.

Altogether, three simulations have been performed to allow a systematic investigation of the correction methods. Without exception, all the simulations were able to stabilize a lifted flame within the computational domain. This was a consequence of the well prediction of the underlying main phenomena, i.e. dispersion and heat and mass transfer of droplets, as well as the turbulent gaseous flow and the flame characteristics. As the investigated methods are able to modify the mixture formation, different shapes were obtained for the simulated flames. But these are rather equivalent and a greater distinction among methods was noticed in specific quantities of dispersed and carrier phases.

Comparisons of the simulation results with experimental data of velocity components of the gaseous phase attest the high quality of the performed LES. Deviations

between both correction methods are negligible, but these are noticed between simulations applying and omitting such methods. The deviations emerge in the flame region, as methods are activated in reaction zones.

As expected, the droplet size distributions are the most affected data by the correction methods. Comparisons between numerical results and experimental data were decisive to determine the best choice for an approach. In general, the PRJ method overcomes the remaining ones, in agreement with the previous outcomes obtained in Dressler et al. [10] for piloted turbulent spray flames. Regardless, the necessity of including a knockdown factor by the effective thickening factor, defined by the STD or the PRJ methods, was evident. Deviations between calculations and measurements are justified by the resulting flame structure.

Although focus was concentrated on the role played by the correction methods, the prediction capability of the flame structure was analyzed in terms of the flame height and shape. It was possible to obtain that the flame height is directly affected by the evaporation correction, being one of the possible reasons to elevate the flame by 12%. Such a result undoubtedly attest the influence of the correction models on the flame structure. In specific the leading edge of the flame, a special region for the conducted investigations. However, none of the three simulations was able to deliver a good adherence with the measured flame height. Such deviations were assigned to two main aspects: the numerical spray injector and the absence of heat losses. As previously posed, prior to the start of the present study, it was decided to use the same injector as the one employed by Both [4], in order to better communicate the obtained outcomes with other works in the literature (e.g. [4, 33]). Improvements of the numerical spray injector and the inclusion of heat losses on boundary conditions, as well as through the evaporative cooling are outlines of this work. Besides this, the consideration of models capable to predict the occurrence of simultaneous flame modes is desirable for future works.

Acknowledgements

We acknowledge the financial support from Coordenação de Aperfeiçoamento de Pessoal de Nível Superior—Brasil (CAPES) - Finance Code 001. We also acknowledge the Santos Dumont (SDumont) supercomputer for providing the high-performance computational infrastructure that enabled this research, particularly in advancing artificial intelligence and scientific simulations. Finally, we extend our sincere thanks to Bruno Renou for the important discussions and for providing the experimental data that supported this work.

Funding

This work was supported by the Coordenação de Aperfeiçoamento de Pessoal de Nível Superior—Brasil (CAPES) under Finance Code 001. The funding was awarded to Satoshi Kuramoto, Luís Eduardo de Albuquerque Paixão e Freire de Carvalho, and Fernando Luiz Sacomano Filho.

References

[1] Crowe, C.T., Sharma, M.P., Stock, D.E.: The particle-source-in cell (psi-cell) model for gas-droplet flows. Journal of Fluids Engineering **99**(2), 325–332 (1977) https://doi.org/10.1115/1.3448756

[2] Boileau, M.: Simulation aux grandes échelles de l'allumage diphasique des foyers aéronautiques. PhD thesis, Institut National Polytechnique, Toulouse, France (2007). https://theses.hal.science/tel-00282523

[3] Boileau, M., Staffelbach, G., Cuenot, B., Poinsot, T., Bérat, C.: Les of an ignition sequence in a gas turbine engine. Combustion and Flame **154**(1), 2–22 (2008) https://doi.org/10.1016/j.combustflame.2008.02.006

[4] Both, A.: Rans-fgm simulation of n-heptane spray flame in openfoam. Master's thesis, Technische Universiteit Delft, Delft, Netherlands (2017)

[5] Broatch, A., Carreres, M., García-Tíscar, J., Belmar-Gil, M.: Spectral analysis and modelling of the spray liquid injection in a lean direct injection (ldi) gas turbine combustor through eulerian-lagrangian large eddy simulations. Aerospace Science and Technology **118**, 106992 (2021) https://doi.org/10.1016/j.ast.2021.106992

[6] Chrigui, M., Gounder, J., Sadiki, A., Masri, A.R., Janicka, J.: Partially premixed reacting acetone spray using les and fgm tabulated chemistry. Combustion and Flame **159**(8), 2718–2741 (2012) https://doi.org/10.1016/j.combustflame.2012.03.009 . Special Issue on Turbulent Combustion

[7] Chrigui, M., Masri, A.R., Sadiki, A., Janicka, J.: Large eddy simulation of a polydisperse ethanol spray flame. Flow, Turbulence and Combustion **90**(4), 813–832 (2013) https://doi.org/10.1007/s10494-013-9449-9

[8] Coussement, A., Schmitt, T., Fiorina, B.: Filtered tabulated chemistry for non-premixed flames. Proceedings of the Combustion Institute **35**(2), 1183–1190 (2015) https://doi.org/10.1016/j.proci.2014.06.010

[9] Dillon, S., Mercier, R., Fiorina, B.: Modelling turbulent multi-regime combustion in les with filtered tabulated chemistry. Combustion and Flame **286**, 114802 (2026) https://doi.org/10.1016/j.combustflame.2026.114802

[10] Dressler, L., Sacomano Filho, F.L., Sadiki, A., Janicka, J.: Influence of thickening factor treatment on predictions of spray flame properties using the atf model and tabulated chemistry. Flow, Turbulence and Combustion **106**, 419–451 (2021) https://doi.org/10.1007/s10494-020-00149-7

[11] Dressler, L., Sacomano Filho, F.L., Ries, F., Nicolai, H., Janicka, J., Sadiki, A.: Numerical prediction of turbulent spray flame characteristics using the filtered

eulerian stochastic field approach coupled to tabulated chemistry. Fluids **6**(2) (2021) https://doi.org/10.3390/fluids6020050

[12] Franzelli, B., Riber, E., Cuenot, B.: Impact of the chemical description on a large eddy simulation of a lean partially premixed swirled flame. Comptes Rendus Mécanique **341**(1), 247–256 (2013) https://doi.org/10.1016/j.crme.2012.11.007 . Combustion, spray and flow dynamics for aerospace propulsion

[13] Franzelli, B., Vié, A., Ihme, M.: Characterizing spray flame–vortex interaction: A spray spectral diagram for extinction. Combustion and Flame **163**, 100–114 (2016) https://doi.org/10.1016/j.combustflame.2015.09.006

[14] Hannebique, G., Sierra, P., Riber, E., Cuenot, B.: Large eddy simulation of reactive two-phase flow in an aeronautical multipoint burner. Flow, Turbulence and Combustion **90**(2), 449–469 (2013) https://doi.org/10.1007/s10494-012-9416-x

[15] Heye, C., Raman, V., Masri, A.R.: Les/probability density function approach for the simulation of an ethanol spray flame. Proceedings of the Combustion Institute **34**(1), 1633–1641 (2013) https://doi.org/10.1016/j.proci.2012.06.107

[16] Jenny, P., Roekaerts, D., Beishuizen, N.: Modeling of turbulent dilute spray combustion. Progress in Energy and Combustion Science **38**(6), 846–887 (2012) https://doi.org/10.1016/j.pecs.2012.07.001

[17] Jones, W.P., Marquis, A.J., Noh, D.: Les of a methanol spray flame with a stochastic sub-grid model. Proceedings of the Combustion Institute **35**(2), 1685–1691 (2015) https://doi.org/10.1016/j.proci.2014.06.086

[18] Klimenko, A.Y., Bilger, R.W.: Conditional moment closure for turbulent combustion. Progress in Energy and Combustion Science **25**, 595–687 (1999) https://doi.org/10.1016/S0360-1285(99)00006-4

[19] Knudsen, E., Shashank, Pitsch, H.: Modeling partially premixed combustion behavior in multiphase les. Combustion and Flame **162**(1), 159–180 (2015) https://doi.org/10.1016/j.combustflame.2014.07.013

[20] Kuenne, G., Ketelheun, A., Janicka, J.: Les modeling of premixed combustion using a thickened flame approach coupled with fgm tabulated chemistry. Combustion and Flame **158**(9), 1750–1767 (2011) https://doi.org/10.1016/j.combustflame.2011.01.005

[21] Kuenne, G., Seffrin, F., Fuest, F., Stahler, T., Ketelheun, A., Geyer, D., Janicka, J., Dreizler, A.: Experimental and numerical analysis of a lean premixed stratified burner using 1d raman/rayleigh scattering and large eddy simulation. Combustion and Flame **159**(8), 2669–2689 (2012) https://doi.org/10.1016/j.combustflame.2012.02.010

[22] Letty, C., Renou, B., Reveillon, J., Saengkaew, S., Gréhan, G.: Experimental study of droplet temperature in a two-phase heptane/air v-flame. Combustion and Flame **160**(9), 1803–1811 (2013) https://doi.org/10.1016/j.combustflame.2013.03.017

[23] Mastorakos, E., Baritaud, T.A., Poinsot, T.J.: Numerical simulations of autoignition in turbulent mixing flows. Combustion and Flame **109**(1), 198–223 (1997) https://doi.org/10.1016/S0010-2180(96)00149-6

[24] Mastorakos, E.: Forced ignition of turbulent spray flames. Proceedings of the Combustion Institute **36**(2), 2367–2383 (2017) https://doi.org/10.1016/j.proci.2016.08.044

[25] Mercier, R., Auzillon, P., Moureau, V., Darabiha, N., Gicquel, O., Veynante, D., Fiorina, B.: Les modeling of the impact of heat losses and differential diffusion on turbulent stratified flame propagation: Application to the tu darmstadt stratified flame. Flow, Turbulence and Combustion **93**(2), 349–381 (2014) https://doi.org/10.1007/s10494-014-9550-8

[26] Pope, S.B.: Pdf methods for turbulent reactive flows. Progress in Energy and Combustion Science **11**(2), 119–192 (1985) https://doi.org/10.1016/0360-1285(85)90002-4

[27] Sacomano Filho, F.L., Chrigui, M., Sadiki, A., Janicka, J.: Les-based numerical analysis of droplet vaporization process in lean partially premixed turbulent spray flames. Combustion Science and Technology **186**(4-5), 435–452 (2014) https://doi.org/10.1080/00102202.2014.883207

[28] Sacomano Filho, F.L., Kuenne, G., Chrigui, M., Sadiki, A., Janicka, J.: A consistent artificially thickened flame approach for spray combustion using les and the fgm chemistry reduction method: Validation in lean partially pre-vaporized flames. Combustion and Flame **184**, 68–89 (2017) https://doi.org/10.1016/j.combustflame.2017.05.031

[29] Sacomano Filho, F.L., Dressler, L., Hosseinzadeh, A., Sadiki, A., Krieger Filho, G.C.: Investigations of evaporative cooling and turbulence flame interaction modeling in ethanol turbulent spray combustion using tabulated chemistry. Fluids **4**(4) (2019) https://doi.org/10.3390/fluids4040187

[30] Sacomano Filho, F.L., Hosseinzadeh, A., Sadiki, A., Janicka, J.: On the interaction between turbulence and ethanol spray combustion using a dynamic wrinkling model coupled with tabulated chemistry. Combustion and Flame **215**, 203–220 (2020) https://doi.org/10.1016/j.combustflame.2020.01.038

[31] Sekularac, N., Lesaffre, T., Laera, D., Gicquel, L.: Large eddy simulations of n-heptane and n-dodecane binary blends in swirling multi-component spray flames. Proceedings of the Combustion Institute **40**(1), 105201 (2024) https://doi.org/

10.1016/j.proci.2024.105201

[32] Shum-Kivan, F., Marrero Santiago, S.J., Verdier, A., Riber, E., Renou, B., Cabot, G., Cuenot, B.: Experimental and numerical analysis of a turbulent spray flame structure. Proceedings of the Combustion Institute **36**, 2567–2575 (2017) https://doi.org/10.1016/j.proci.2016.06.039

[33] Sitte, M.P., Mastorakos, E.: Large eddy simulation of a spray jet flame using doubly conditional moment closure. Combustion and Flame **199**, 309–323 (2019) https://doi.org/10.1016/j.combustflame.2018.08.026

[34] Tyliszczak, A., Cavaliere, D.E., Mastorakos, E.: Les/cmc of blow-off in a liquid fueled swirl burner. Flow, Turbulence and Combustion **92**(1), 237–267 (2014) https://doi.org/10.1007/s10494-013-9477-5

[35] Ukai, S., Kronenburg, A., Stein, O.T.: Large eddy simulation of dilute acetone spray flames using cmc coupled with tabulated chemistry. Proceedings of the Combustion Institute **35**(2), 1667–1674 (2015) https://doi.org/10.1016/j.proci.2014.06.013

[36] Verdier, A., Marrero Santiago, J., Vandel, A., Saengkaew, S., Cabot, G., Grehan, G., Renou, B.: Experimental study of local flame structures and fuel droplet properties of a spray jet flame. Proceedings of the Combustion Institute **36**(2), 2595–2602 (2017) https://doi.org/10.1016/j.proci.2016.07.016

[37] Verdier, A.: Experimental study of dilute spray combustion. PhD thesis, Normandie Université, Rouen, France (2017)

[38] Verdier, A., Marrero Santiago, J., Vandel, A., Godard, G., Cabot, G., Renou, B.: Local extinction mechanisms analysis of spray jet flame using high speed diagnostics. Combustion and Flame **193**, 440–452 (2018) https://doi.org/10.1016/j.combustflame.2018.03.032

[39] Wen, J., H., Y., Nishiie, T., Iino, J., M., A., Kurose, R.: A flamelet les of turbulent dense spray flame using a detailed high-resolution vof simulation of liquid fuel atomization. Combustion and Flame **237**, 111742 (2022) https://doi.org/10.1016/j.combustflame.2021.111742

[40] Fredrich, D., Giusti, A.: Numerical investigation of multi-component droplet evaporation and autoignition for aero-engine applications. Combustion and Flame **241**, 112023 (2022) https://doi.org/10.1016/j.combustflame.2022.112023

[41] Krieger Filho, G.C., Silva, F.M.F., Pacífico, A.L., Sacomano Filho, F.L., Zabeu, C.B., Nigro, F.B., França, O.M., Penaranda, A., Lacava, P.T.: Extended coherent flame model applied to an optical single-cylinder engine fueled with ethanol. Applied Thermal Engineering **236**, 121399 (2024) https://doi.org/10.1016/j.applthermaleng.2023.121399

[42] Prosperetti, A., Tryggvason, G.: Computational Methods for Multiphase Flow. Cambridge University Press, ??? (2007)

[43] Neophytou, A., Mastorakos, E.: Simulations of laminar flame propagation in droplet mists. Combustion and Flame **156**(8), 1627–1640 (2009) https://doi.org/10.1016/j.combustflame.2009.02.014

[44] Sacomano Filho, F.L., L. E. A. P. F. Carvalho, van Oijen, J.A., Krieger Filho, G.C.: Effects of reaction mechanisms and differential diffusion in oxy-fuel combustion including liquid water dilution. Fluids **6**(2) (2021) https://doi.org/10.3390/fluids6020047

[45] Shastry, V., Cazeres, Q., Rochette, B., Riber, E., Cuenot, B.: Numerical study of multicomponent spray flame propagation. Proceedings of the Combustion Institute **38**(2), 3201–3211 (2021) https://doi.org/10.1016/j.proci.2020.07.090

[46] Sacomano Filho, F.L., Freire de Carvalho, L.E., Carvalho Santos, A., Vié, A., van Oijen, J.A.: Impact of multi-component description of hydrophilic fuel droplets in propagating spray flames. Combustion and Flame **263**, 113415 (2024) https://doi.org/10.1016/j.combustflame.2024.113415

[47] Portela, L.M., Oliemans, R.V.A.: Eulerian–lagrangian dns/les of particle–turbulence interactions in wall-bounded flows. International Journal for Numerical Methods in Fluids **43**(9), 1045–1065 (2003) https://doi.org/10.1002/fld.616

[48] Fiorina, B., Vicquelin, R., Auzillon, P., Darabiha, N., Gicquel, O., Veynante, D.: A filtered tabulated chemistry model for les of premixed combustion. Combustion and Flame **157**(3), 465–475 (2010) https://doi.org/10.1016/j.combustflame.2009.09.015

[49] Auzillon, P., Gicquel, O., Darabiha, N., Veynante, D., Fiorina, B.: A filtered tabulated chemistry model for les of stratified flames. Combustion and Flame **159**(8), 2704–2717 (2012) https://doi.org/10.1016/j.combustflame.2012.03.006 . Special Issue on Turbulent Combustion

[50] Butler, T.D., O'Rourke, P.J.: A numerical method for two dimensional unsteady reacting flows. Symposium (International) on Combustion **16**, 1503–1515 (1977) https://doi.org/10.1016/S0082-0784(77)80432-3

[51] Colin, O., Ducros, F., Veynante, D., Poinsot, T.: A thickened flame model for large eddy simulations of turbulent premixed combustion. Physics of Fluids **12**(7), 1843–1863 (2000) https://doi.org/10.1063/1.870436

[52] Durand, L., Polifke, W.: Implementation of the thickened flame model for large eddy simulation of turbulent premixed combustion in a commercial solver. Turbo Expo: Power for Land, Sea, and Air **2**, 869–878 (2007)

[53] Poncet, S., Mehl, C., Truffin, K., Colin, O.: A thickened flame model adaptation to weakly stretched flames for non-unity lewis number mixtures. Combustion and Flame **270**, 113758 (2024) https://doi.org/10.1016/j.combustflame.2024.113758

[54] O'Rourke, P.J., Bracco, F.V.: Two scaling transformations for the numerical computation of multidimensional unsteady laminar flames. Journal of Computational Physics **33**(2), 185–203 (1979) https://doi.org/10.1016/0021-9991(79)90015-9

[55] Weller, H.G., Tabor, G., Jasak, H., Fureby, C.: A tensorial approach to computational continuum mechanics using object orientated techniques. Computers in Physics **12**, 620–631 (1998) https://doi.org/10.1063/1.168744

[56] Ries, F., Obando, P., Shevchuck, I., Janicka, J., Sadiki, A.: Numerical analysis of turbulent flow dynamics and heat transport in a round jet at supercritical conditions. International Journal of Heat and Fluid Flow **66**, 172–184 (2017) https://doi.org/10.1016/j.ijheatfluidflow.2017.06.007

[57] Toda, H., Cabrit, O., Balarac, G., Bose, S., Lee, J., Choi, H., Franck, N.: A subgrid-scale model based on singular values for les in complex geometries. Proc. Summer Program (2010)

[58] van Oijen, J.A., de Goey, L.P.H.: Modelling of premixed laminar flames using flamelet-generated manifolds. Combustion science and technology **161**, 113–137 (2000) https://doi.org/10.1080/00102200008935814

[59] van Oijen, J.A., Donini, A., Bastiaans, R.J.M., ten Thije Noonkkamp, J.H.M., de Goey, L.P.H.: State-of-the-art in premixed combustion modeling using flamelet generated manifolds. Progress in Energy and Combustion Science **57**, 30–74 (2016) https://doi.org/10.1016/j.pecs.2016.07.001

[60] Somers, B.: The simulation of flat flames with detailed and reduced chemical models. Master's thesis, Technische Universiteit Eindhoven, Eindhoven, Netherlands (1994)

[61] Ranzi, E., Frassoldati, A., Stagni, A., Pelucchi, M., Cuoci, A., Faravelli, T.: Reduced kinetic schemes of complex reaction systems: Fossil and biomass-derived transportation fuels. International Journal of Chemical Kinetics **46**(9), 512–542 (2014) https://doi.org/10.1002/kin.20867

[62] Ranzi, E., Cavallotti, C., Cuoci, A., Frassoldati, A., Pelucchi, M., Faravelli, T.: New reaction classes in the kinetic modeling of low temperature oxidation of n-alkanes. Combustion and Flame **162**(5), 1679–1691 (2015) https://doi.org/10.1016/j.combustflame.2014.11.030

[63] Bagheri, G., Ranzi, E., Pelucchi, M., Parente, A., Frassoldati, A., Faravelli, T.: Comprehensive kinetic study of combustion technologies for low environmental impact: Mild and oxy-fuel combustion of methane. Combustion and Flame **212**,

142–155 (2020) https://doi.org/10.1016/j.combustflame.2019.10.014

[64] Bilger, R.W.: The structure of turbulent nonpremixed flames. Symposium (International) on Combustion **22**, 475–488 (1989) https://doi.org/10.1016/S0082-0784(89)80054-2

[65] Charlette, F., Meneveau, C., Veynante, D.: A power-law flame wrinkling model for LES of premixed turbulent combustion part I: non-dynamic formulation and initial tests. Combustion and Flame **131**, 159–180 (2002) https://doi.org/10.1016/S0010-2180(02)00400-5

[66] Charlette, F., Meneveau, C., Veynante, D.: A power-law flame wrinkling model for LES of premixed turbulent combustion part II: dynamic formulation. Combustion and Flame **131**, 181–197 (2002) https://doi.org/10.1016/S0010-2180(02)00401-7

[67] Aschmoneit, K.: Numerische beschreibung technischer verbrennungssysteme. PhD thesis, Technische Universität Darmstadt, Darmstadt, Germany (2013)

[68] Abramzon, B., Sirignano, W.A.: Droplet vaporization model for spray combustion calculations. International Journal of Heat and Mass Transfer **32**, 1605–1618 (1989) https://doi.org/10.1016/0017-9310(89)90043-4

[69] Miller, R.S., Harstad, K., Bellan, J.: Evaluation of equilibrium and non-equilibrium evaporation models for many-droplet gas-liquid flow simulations. International Journal of Multiphase Flow **24**, 1025–1055 (1998) https://doi.org/10.1016/j.combustflame.2011.01.005

[70] Mulla, I.A., Godard, G., Cabot, G., Grisch, F., Renou, B.: Quantitative imaging of nitric oxide concentration in a turbulent n-heptane spray flame. Combustion and Flame **203**, 217–229 (2019) https://doi.org/10.1016/j.combustflame.2019.02.005

[71] Yamashita, H., Kushida, G., Takeno, T.: A numerical study of the transition of jet diffusion flames. Proceedings: Mathematical and Physical Sciences **431**, 301–314 (1990)

Supplementary Files

This is a list of supplementary files associated with this preprint. Click to download.

- supplemetarymaterial.pdf
- supplementary.zip